



## Yeast-based assays for the high-throughput screening of inhibitors of coronavirus RNA cap guanine-N7-methyltransferase



Ying Sun<sup>a</sup>, Zidao Wang<sup>a</sup>, Jiali Tao<sup>a</sup>, Yi Wang<sup>a</sup>, Andong Wu<sup>a</sup>, Ziwen Yang<sup>b</sup>, Kaimei Wang<sup>b</sup>, Liqiao Shi<sup>b</sup>, Yu Chen<sup>a,\*</sup>, Deyin Guo<sup>a,\*</sup>

<sup>a</sup>State Key Laboratory of Virology, College of Life Sciences, Wuhan University, Wuhan 430072, PR China

<sup>b</sup>Biological Pesticide Engineering Research Center, Hubei Academy of Agricultural Science, Hubei 430072, PR China

### ARTICLE INFO

#### Article history:

Received 14 September 2013

Revised 29 January 2014

Accepted 3 February 2014

Available online 11 February 2014

#### Keywords:

Coronavirus

nsp14

N7-methyltransferase

Inhibitor

Yeast

Sinefungin

### ABSTRACT

The 5'-cap structure is a distinct feature of eukaryotic mRNAs and is important for RNA stability and protein translation by providing a molecular signature for the distinction of self or non-self mRNA. Eukaryotic viruses generally modify the 5'-end of their RNAs to mimic the cellular mRNA structure, thereby facilitating viral replication in host cells. However, the molecular organization and biochemical mechanisms of the viral capping apparatus typically differ from its cellular counterpart, which makes viral capping enzymes attractive targets for drug discovery. Our previous work showed that SARS coronavirus (SARS-CoV) non-structural protein 14 represents a structurally novel and unique guanine-N7-methyltransferase (N7-MTase) that is able to functionally complement yeast cellular N7-MTase. In the present study, we developed a yeast-based system for identifying and screening inhibitors against coronavirus N7-MTase using both 96-well and 384-well microtiter plates. The MTase inhibitors previously identified by *in vitro* biochemical assays were tested, and some, such as sinefungin, effectively suppressed N7-MTase in the yeast system. However, other compounds, such as ATA and AdoHcy, did not exert an inhibitory effect within a cellular context. These results validated the yeast assay system for inhibitor screening yet also demonstrated the difference between cell-based and *in vitro* biochemical assays. The yeast system was applied to the screening of 3000 natural product extracts, and three were observed to more potently inhibit the activity of coronavirus than human N7-MTase.

© 2014 Elsevier B.V. All rights reserved.

### 1. Introduction

The cellular messenger RNAs (mRNAs) of higher eukaryotes and many viral RNAs are sequentially methylated at the N-7 and 2'-O positions of the 5'-guanosine cap. The cap structure has several important biological roles, such as protecting mRNA from degradation by 5'-3' exoribonucleases (Schwer et al., 1998) and directing pre-mRNA splicing and mRNA export from the nucleus (Darnell, 1979). In addition, the cap structure confers stability to mRNAs and ensures their efficient recognition by translation initiation factor 4F for translation (Filipowicz et al., 1976; Schibler and Perry,

1977). In contrast, host and virus RNA molecules with unprotected 5'-ends are degraded in cytoplasmic compartments (Liu and Kiledjian, 2006). Uncapped RNAs, such as nascent viral transcripts, may also be detected as "non-self" by the RNA sensors RIG-I, Mda-5, and IFIT in host cells (Abbas et al., 2013; Bowzard et al., 2013; Hornung et al., 2006; Züst et al., 2011), triggering antiviral innate immune responses through the production of interferon or IFIT (interferon-induced protein)-mediated antiviral activity (Daffis et al., 2010; Nallagatla et al., 2008; Rehwinkel et al., 2010).

The following four cap-forming enzymes are involved in the formation of the cap-1 structure. (i) RNA triphosphatase hydrolyzes the 5'-triphosphate of nascent pre-mRNA to a 5'-diphosphate. (ii) RNA guanylyltransferase caps the diphosphate RNA with GMP. (iii) RNA guanine-N7-methyltransferase (N7-MTase) methylates the GpppN cap at the N7 position of guanine, resulting in the cap-0 structure (m7GpppN) (Shuman, 2001). (iv) Ribose 2'-O-MTase further methylates the first nucleotide of higher eukaryotic cellular and viral mRNAs at the ribose 2'-OH position to form cap-1 (m7GpppNm) structures (Furuichi and Shatkin, 2000). Both N7 and 2'-O-MTases utilize S-adenosyl-L-methionine (AdoMet) as a methyl

**Abbreviations:** SARS, severe acute respiratory syndrome; SARS-CoV, SARS coronavirus; nsp, nonstructural protein; N7-MTase, guanine-N7-methyltransferase; 2'-O-MTase, 2'-O-methyltransferase; AdoMet, S-adenosyl-L-methionine; AdoHcy, S-adenosyl-L-homocysteine; ATA, aurintricarboxylic acid; IC<sub>50</sub>, inhibitory concentration at 50% activity.

\* Corresponding authors. Tel.: +86 27 87884604 (Y. Chen), +86 27 68752506 (D. Guo).

E-mail addresses: [chenyu@whu.edu.cn](mailto:chenyu@whu.edu.cn) (Y. Chen), [dguo@whu.edu.cn](mailto:dguo@whu.edu.cn) (D. Guo).

donor and generate *S*-adenosyl-L-homocysteine (AdoHcy) as a by-product.

Eukaryotic viruses that replicate in the cytoplasm encode their own capping apparatus, and the structure and mechanisms of the viral RNA capping apparatus are different from those of host cells (Furuichi and Shatkin, 2000), which could be useful for the development of antiviral drugs. Indeed, a number of biochemical and functional studies have previously addressed methyltransferases as potential inhibitor targets (Chrebet et al., 2005; Schwer et al., 2001; Woyciniuk et al., 1995). Moreover, the enzymes involved in the coronavirus capping pathway are increasingly considered to be promising targets for potential anti-coronavirus drugs (Bouvet et al., 2010).

Coronaviruses (CoVs), infect many species of animals, including humans, and cause acute or chronic respiratory diseases (e.g., severe acute respiratory syndrome coronavirus [SARS-CoV], Middle East respiratory syndrome coronavirus [MERS-CoV] (de Groot et al., 2013; Zaki et al., 2012), and infectious bronchitis virus [IBV], enteric diseases (e.g., transmissible gastroenteritis virus [TGEV]), and central nervous system (CNS) diseases (murine hepatitis virus [MHV]) (Weiss and Navas-Martin, 2005). CoVs are the largest RNA viruses, are enveloped, and contain a single-stranded, positive-sense RNA genome ranging from 27 to 31.5 kb in length. The genome of SARS-CoV contains 14 open reading frames (ORFs) (Snijder et al., 2003) and generates 16 nonstructural proteins (nsps) produced by the autocatalytic processing of the polyprotein by 2 viral proteases (Ziebuhr et al., 2000). CoVs replicate in the host cytoplasm and encode their own capping enzymes. Among the four capping enzymes involved in coronavirus m7GpppAm-cap formation, guanine-N7-methyltransferase (N7-MTase) was identified as nsp14 in our previous work using a yeast genetic system (Chen et al., 2009), and 2'-*O*-methyltransferase (2'-*O*-MTase) is formed by nsp16 with nsp10 as a cofactor (Chang et al., 2011; Chen et al., 2011; Decroly et al., 2011; Lugari et al., 2010). SARS-coronavirus nsp14 was previously characterized as a 3'- to 5'-exoribonuclease (ExoN) (Chen et al., 2007; Minskaia et al., 2006), and the N7-MTase domain was mapped to the carboxy-terminal part of the protein (Chen et al., 2009). Interestingly, the ExoN active site is dispensable, though the ExoN domain is required for N7-MTase activity. The combination of the two functional domains (Chen et al., 2009, 2013), a unique feature among all N7-MTases, indicates that SARS-CoV N7-MTase is a novel form of RNA-processing enzyme and thus suggests it as an attractive target for the development of antiviral drugs.

It has been shown that the capping functions in yeast cells can be replaced by the cap-forming enzymes of mammals or DNA viruses (Ho et al., 2000; Saha et al., 1999, 2003), and we previously found that coronavirus nsp14 could replace yeast cap N7-MTase in vivo (Chen et al., 2009, 2013). In the present study, we further developed the yeast genetic system as a high-throughput enzymatic activity assay platform of various N7-MTases to identify coronavirus N7-MTase inhibitors. The system was validated using MTase inhibitors previously identified by in vitro biochemical assays and then used for the screening of 3000 natural product extracts.

## 2. Materials and methods

### 2.1. Construction of yeast and *Escherichia coli* expression plasmids

The coding sequences of nonstructural protein 14 of SARS-CoV, MHV, TGEV, and IBV were PCR amplified from cDNAs of the SARS-CoV WHU strain (GenBank accession No. AY394850) (Hussain et al., 2005), MHV-A59 (GenBank accession No. AY700211.1), TGEV (GenBank accession No. FJ755618.2), and IBV (GenBank accession No. AJ311317.1) and inserted into the BamHI and XhoI sites of the yeast vector pMceK294A (2  $\mu$ m, TRP1) (Chen et al., 2009).

The cDNA of MERS-CoV nsp14 was chemically synthesized according to the deposited sequence of MERS-CoV (GenBank accession No. KF192507.1) and cloned into pMceK294A. For expression in *E. coli* cells, the coding sequences of SARS and MHV nsp14 were inserted into the NdeI and SalI sites of pET30a, and TGEV nsp14 (kindly provided by Dr. Luis. Enjuanes) was cloned into the BamHI and SalI sites of pETduet-1. The plasmid for IBV expression (pDest14-IBV-nsp14) was a kind gift from Dr. Eric J. Snijder.

### 2.2. Protein expression and purification

*E. coli* BL21 (DE3) cells (Novagen) were separately transformed with the pET30a-SARS-nsp14, pET30a-MHV-nsp14, pET-duet1-TGEV-nsp14, and pDest14-IBV-nsp14 plasmids. The cells were cultured at 37 °C in 1 L of LB medium supplemented with kanamycin (50  $\mu$ g/ml) or ampicillin (100  $\mu$ g/ml) until the culture density ( $A_{600}$ ) reached 0.6–0.8 and then induced with 0.5 mM isopropyl- $\beta$ -D-1-thiogalactopyranoside (IPTG) for 20 h at 16 °C. The cells were harvested, and the recombinant proteins were purified by affinity chromatography using previously described protocols (Chen et al., 2007). The protein was concentrated by ultra-filtration (Millipore), and the buffer was changed to 20 mM Tris-HCl (pH 8.0), 150 mM NaCl, 20% glycerol, and 0.2 mM DTT. The protein was stored at -70 °C until use.

### 2.3. Biochemical assay for N7 methylation and suppression

N7-MTase activity assays were carried out in a 30- $\mu$ L reaction mixture (40 mM Tris-HCl [pH 7.5], 2 mM MgCl<sub>2</sub>, 2 mM DTT, 40 units RNase inhibitor, 0.01 mM SAM) with 1  $\mu$ Ci of *S*-adenosyl [methyl-<sup>3</sup>H] methionine (67.3 Ci/mmol, 0.5 mCi/ml). The purified coronavirus nsp14 proteins were added at a final concentration of 200 nM using 0.5 mM GpppA cap analog as the substrate. After incubation at 37 °C for 1.5 h, the reaction was stopped by adding an equal volume of stop solution (0.2% SDS and 20 mM EDTA). The samples were purified using DEAE-Sephadex columns, and the methylation of the RNA substrates was quantitated in counts per minute (cpm) using a Scintillation Counter (Beckman Coulter LS 6500).

To measure the inhibitory effects of coronaviral N7-MTase activity, AdoHcy, Aurintricarboxylic acid (ATA), ribavirin, and sinefungin were used at a maximum concentration of 100  $\mu$ M in the assays. Typically, the enzyme and GpppA substrate were pre-incubated with each compound at room temperature (RT) for 20 min, and the reactions were initiated by the addition of *S*-adenosyl [methyl-<sup>3</sup>H] methionine. A control reaction was performed in the presence of 1% DMSO instead of each tested compound. The IC<sub>50</sub> (concentration of the drug to repress 50% of the N7-MTase activity) value of sinefungin against SARS-CoV nsp14 was determined using GraphPad Prism5. The data were adjusted to a logistic dose-response function.

### 2.4. N7-MTase activity assays in a yeast-based system

The yeast N7-MTase gene *Abd1* has been shown to be essential for yeast cell growth (Mao et al., 1995). *Saccharomyces cerevisiae* strain YBS40 (MATa leu2 ade2 trp1 his3 ura3 can1 abd1::hisGp360-ABD1) (Mao et al., 1995) was transformed with yeast expression plasmids carrying coronavirus nsp14 and human N7-MTase (pYX232-HCM1) as a positive control (Chen et al., 2009; Saha et al., 1999). Trp<sup>+</sup> transformants were selected at 30 °C on an agar medium lacking tryptophan. The cells were then streaked onto an agar medium lacking tryptophan and containing 0.75 mg/ml of 5-fluoroorotic acid (5-FOA) (Sikorski and Boeke, 1991) at 30 °C for up to 5 days to counter-select the URA3<sup>+</sup> plasmid carrying the yeast *Abd1* gene. The formation of FOA-resistant colonies indicated that the

transformation of the mutants could replace or complement the endogenous cap N7-methyltransferase function residing in the URA3 plasmid (Chen et al., 2009, 2013).

A solution of sinefungin (adenosylornithine, CALBioCHEM 5670-51), ribavirin (1- $\beta$ -D-ribofuranosyl-1,2,4-triazole-3-carboxamide, Sigma R-9644), and AdoHcy (adenosine-homocysteine, Sigma A-9384) was prepared in H<sub>2</sub>O or DMSO (Decroly et al., 2008; Luzhkov et al., 2007; Milani et al., 2009). ATA (aurintricarboxylic acid, Sigma A-1895) was dissolved in 0.1 mM NaOH (Decroly et al., 2008). Concentrations of the stock solutions were set to 10 mM, and the compounds were stored at  $-20^{\circ}\text{C}$ .

Microtiter plates (96- or 384-well plates) were used for the yeast growth suppression test and inhibitor screening. A single transformed colony of the YBS40 strain containing plasmids expressing human N7-MTase (MT-Human), SARS-CoV N7-MTase (MT-SARS), N7-MTases of other coronaviruses (MT-MHV, MT-TGEV, and MT-IBV), and the pMceK294A vector as control (representing the yeast N7-MTase [MT-Yeast]), were inoculated separately into 5 ml of a basic medium (Min SD Base) lacking tryptophan and incubated at  $30^{\circ}\text{C}$  for 21–24 h until reaching a similar final cell density in the stationary phase ( $0.5\text{--}1.0 \times 10^8$  cells/ml) (Chrebet et al., 2005). The starting cell density of the yeast-based assay was  $A_{595} = 0.01$  and contained different inhibitor candidates or 1% DMSO as a negative control. For high-throughput screening, 30  $\mu\text{g/ml}$  or 15  $\mu\text{g/ml}$  natural product extract was added into the 96-well or 384-well microtiter plates. The starting volumes for the 96-well and 384-well microtiter plates were 100  $\mu\text{L}$  and 50  $\mu\text{L}$ , respectively, and the final cell density ( $A_{595}$ ) was measured using a Multifunctional Microplate Reader (Tecan GENios) after incubation for 20 h at  $30^{\circ}\text{C}$  in a shaker.

### 2.5. Quantitative Real-Time PCR

After incubation, yeast cells were collected and then ground in liquid nitrogen. Total RNA was isolated from cells using Trizol reagent (Invitrogen) and subjected to real-time PCR analysis to measure mRNA expression. Real-time PCR was performed using Faststart Universal SYBR Green Mastermix (Roche) and analyzed on 7500 Real Time PCR System (Applied Biosystems). Gene-specific primer sequences are as follows: N7-MTase of the MT-SARS, forward: 5'-GATCATTACTGGTCTTCATCCTACA-3' and reverse: 5'-AATC CACGCACGAACGTGACGAATA-3'; N7-MTase of the MT-Human, forward: 5'-AGCTCAACAGTGGCTGCCATTACA-3' and reverse: 5'-ATC GGCAATATCAGTACAACTAGC-3'; N7-MTase of the MT-Yeast and YBS40, forward: 5'-TGTCACAAGAAGACTATGACCGTCA-3' and reverse: 5'-ATGGATCTATTGCGATCATCTCTA-3'; Beta-actin, forward: 5'-AAGACCAAGGTATCATGGTCCG-3' and reverse: 5'-CGGAAG AGTACAAGGACAAAACGGC-3'.

### 2.6. Preparation of microbial natural product extracts

The microbial natural product extracts were obtained from the microbial natural product library at Hubei Biopesticide Engineering Research Centre (HBERC) and consisted of purified secondary metabolites, semi-purified fractions and extracts from actinomycetes and fungi isolated from soil, lichen, fresh leaves, organic samples, and mushrooms using classical isolation methods. For the soil or lichen, 1 mg was quantified and placed into a tube containing 10 ml of sterilized sodium lauryl sulfate solution and shaken for 1 min. The other samples were seeded aseptically and chopped into small pieces using a blender. The samples were then plated on two different agar media and incubated at  $28^{\circ}\text{C}$  for 7–9 days. The actinomycetes and fungi were isolated to pure culture and incubated at  $28^{\circ}\text{C}$ . The microbial isolates were morphologically characterized, stored and archived. The ratio of actinomycetes/fungi in the collection of microorganisms at HBERC was around 2.5:1.

The microbial identity will be further characterized by classical and molecular methodology when active compounds are identified from the corresponding microbial extracts. For preparation of the microbial extracts, each microbial isolate was fermented in 200 ml fermentation medium and the resulting cultures were extracted with ethyl acetate. For making the working solution of the microbial extracts, the extracts were dissolved in ethanol to a concentration of 1 mg/ml (w/v). In total, 3000 microbial culture extracts were used for MTase inhibitor screening in this study, which were prepared from actinomycetes and fungi.

## 3. Results

### 3.1. Establishment of yeast genetic system-based assays of N7-MTase activity

Our previous study showed that SARS-CoV nsp14 possesses N7-MTase activity that could substitute for cellular N7-MTase in yeast (Chen et al., 2009, 2013). In this system, the gene *Abd1* encoding yeast N7-MTase is knocked out from the yeast genome and complemented by expression of *Abd1* from a plasmid with a URA3 selective marker, resulting in yeast strain YBS40, whereas the exogenous N7-MTase is expressed from another plasmid with a Trp selective marker. The expression of a functional URA3 gene encoding orotidine-5'-monophosphate decarboxylase results in the conversion of the nontoxic 5-FOA compound to toxic 5-fluorouracil in yeast. In a medium containing 5-FOA, which counter-selects URA3-expressing cells, the yeast cells can grow normally only when the exogenous protein can replace the function of the cellular N7-MTase (Fig. 1A). In this study, we confirmed that SARS-CoV and human N7-MTase could rescue the growth of yeast cells that were deficient in N7-MTase. We further tested whether this N7-MTase activity is universal for nsp14 from other coronaviruses. As shown in Fig. 1B, nsp14 from other coronaviruses, including TGEV (group 1), MHV (group 2a), SARS-CoV (group 2b), MERS-CoV (group 2c), and IBV (group 3), showed N7-MTase activity that was functional in vivo by complementing the endogenous yeast enzyme. These results indicate that N7-MTase is well conserved among different coronaviruses and that nsp14 appears to be a target for the development of a universal inhibitor against coronaviruses. We then generated three yeast strains that grew dependently on the N7-MTase activity from SARS-CoV (MT-SARS), humans (MT-human), and yeast (MT-yeast).

To compare the expression levels of these N7-MTases, we analyzed the mRNA levels of the N7-MTases using real-time PCR. As shown in Fig. 1C, there are no significant differences between the mRNA levels of MT-SARS and MT-human, which are under the control of the same yeast *TPI1* promoter. The mRNA of MT-yeast, which was transformed with pMceK294A vector as control, is similar with yeast strain YBS40, because the mRNAs of yeast N7-MTases are transcribed from the complementary plasmids (URA3) bearing the yeast-MT. In the strains with MT-SARS and MT-human, the expression of yeast N7-MTase could not be detected (data not shown). As the expression of MT-SARS and MT-human is at the similar level, these yeast strains could be used to identify the inhibitors that inhibit SARS-CoV MTase more potently than human MTase. However, the mRNA levels of MT-SARS and MT-human are four times higher than that of MT-yeast, the latter being expressed from a low-copy-number plasmid with centromeric element (*Cen*), the inhibitory activity on SARS-CoV and yeast MTases cannot be directly compared.

To establish a drug screening system using these yeast strains, we first tested whether the expression of viral or human N7-MTase influenced yeast growth. Individual colonies of MT-Yeast, MT-Human, and MT-SARS were cultured in a medium lacking tryptophan,

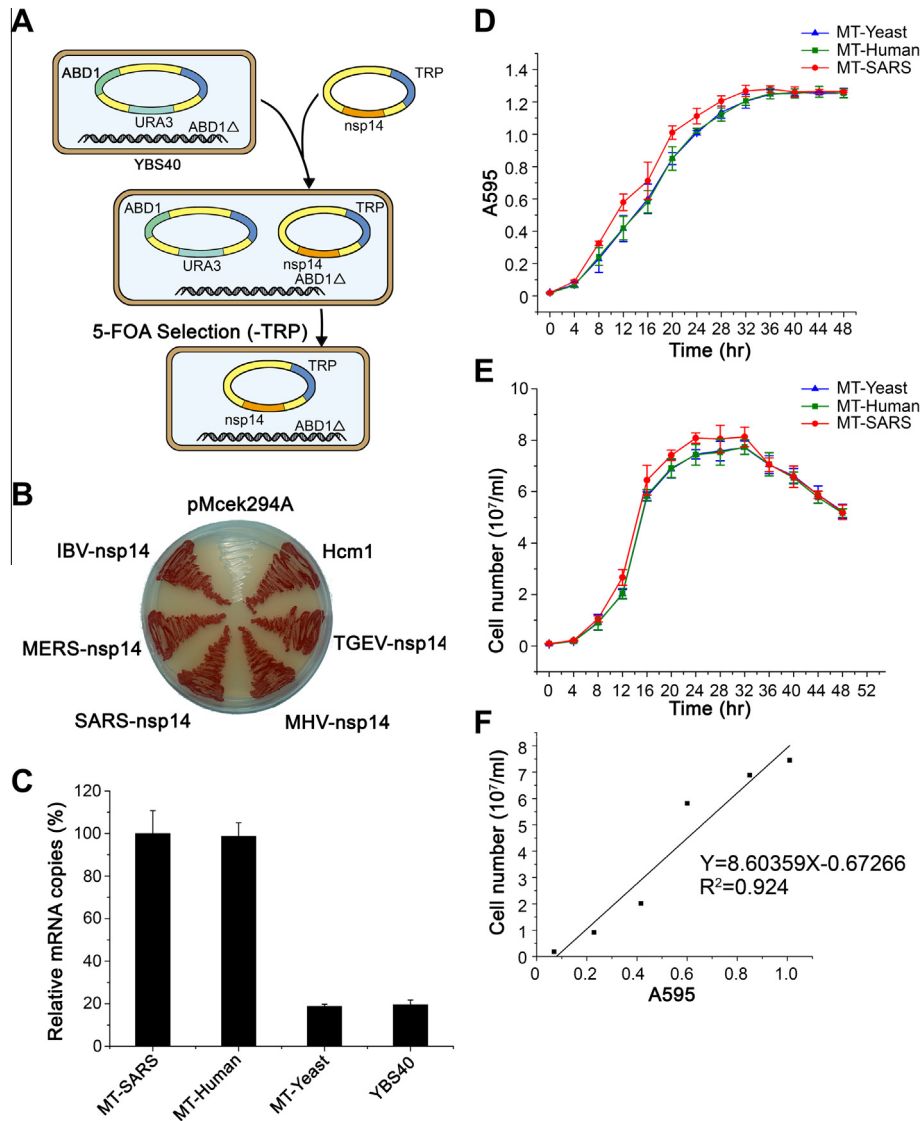


**Fig. 1.** Establishment of a yeast growth system with the substitution of yeast N7-MTase by coronavirus nsp14. (A) Diagram for the replacement of yeast *Abd1* by coronavirus nsp14. In yeast strain YBS40, the chromosomal *Abd1* locus encoding the yeast cap N7-MTase is deleted and the cell growth depends on the maintenance of plasmid p360-ABD1 (URA3) that harbors the *Abd1* gene and URA3 selection marker. The yeast strain YBS40 was transformed with a *TRP1* plasmid carrying the gene of coronavirus nsp14 or human N7-MTase and then placed under 5-FOA selection to counter-select for the URA3 plasmid. The yeast cells only grow when the foreign gene in the *TRP1* plasmid can functionally complement the yeast *Abd1* gene as the plasmid p360-ABD1 (URA3), which is toxic on 5-FOA medium, is lost during the counter-selection. (B) Yeast growth on 5-FOA medium after the replacement of *Abd1* by human HCM1 and coronavirus nsp14 (TGEV-nsp14, MHV-nsp14, SARS-nsp14, MERS-nsp14, and IBV-nsp14), respectively. (C) Relative mRNA transcription levels of the N7-MTases of MT-SARS, MT-Human, MT-Yeast and YBS40.  $\beta$ -actin mRNAs were detected as internal control to show the equal amount of mRNAs used in real-time PCR. The mean values of three independent experiments are shown, and the standard deviations (SD) are indicated by error bars, SD. (D) Growth curve of yeast YBS40 transformed with pMcek294A (MT-Yeast), HCM1 (MT-Human), and SARS-CoV-nsp14 (MT-SARS) plotted by the spectrophotometric measurement of cell density. The strains were cultured in SD/Trp medium in 96-microtiter plates at 30 °C, and a spectrophotometer was used to measure  $A_{595}$  at 4 h-intervals over the course of 48 h. The mean values of three independent experiments are shown, and the standard deviations (SD) are indicated by error bars, SD. (E) Growth curve of the MT-Yeast, MT-Human, and MT-SARS yeast strains were plotted by directly counting the cell number. (F) Positive correlation of optical absorbance of cell culture and cell number during logarithmic growth phase. The least square method was used to evaluate the interrelationships between the two variables (X and Y), where X represents the spectrophotometric measurement ( $A_{595}$ ) and Y represents the corresponding cell number in the logarithmic phase (4–24 h) of MT-SARS. The linear regression equation for the MT-SARS strain,  $y = 8.60359x - 0.67266$  ( $R^2 = 0.924$ ,  $R^2$  is regressive coefficient), was obtained through normative analysis in least square method with Excel program. In this linear regression equation, there is a correlativity between the  $A_{595}$  of culture liquid and cell number in the logarithmic phase (4–24 h) of MT-SARS when the  $R^2 > 0.9$ .

and the pre-cultures were diluted with fresh medium to an  $A_{595} = 0.01$ . A 100- $\mu$ l aliquot of the culture was incubated in each well of two 96-well plates, one of which was used for measuring yeast propagation by spectrophotometry, whereas the other plate was used for the direct counting of the cell number. Measurements were performed at 4-h intervals over 48 h. As shown in Fig. 1D and E, all three yeast strains (MT-SARS, MT-human, and MT-yeast) showed similar growth curves within 48 h, indicating that both the SARS-CoV and human MTases could support the normal growth of yeast

cells. At such a growth condition, starting with a liquid culture at  $A_{595} = 0.01$ , the time period between 4 and 24 h corresponded to the logarithmic growth phase (Fig. 1D and E). During this growth phase, the optical density ( $A_{595}$ ) was well correlated with the cell number as demonstrated for the yeast strain MT-SARS by linear regression analysis (Fig. 1F). In the linear regression equation,  $y = 8.60359x - 0.67266$  ( $R^2 = 0.924$ ,  $R^2$  is regressive coefficient), it shows that there is a correlativity between the  $A_{595}$  of culture liquid and cell number in the logarithmic phase (4–24 h) of MT-SARS when

the  $R^2 > 0.9$ . Similarly, there was also a high correlativity between the two optical absorbance and the cell number for strains MT-Yeast and MT-Human, with linear regression equations  $y = 8.379x - 1.0337$  ( $R^2 = 0.926$ ) and  $y = 8.514x - 0.6286$  ( $R^2 = 0.922$ ), respectively. As spectrophotometric measurements can facilitate rapid and high-throughput evaluation of microtiter plates, the optical density of the cell culture was applied to measure yeast growth in the ensuing experiments.

### 3.2. Verification of the yeast-based assay for identification of N7-MTase inhibitors

To validate the yeast-based system for identifying and screening inhibitors against viral N7-MTases, we tested previously reported MTase inhibitors, including AdoHcy, sinefungin, aurintricarboxylic acid (ATA), and ribavirin (Bouvet et al., 2010). We first detected the N7-MTase activities of coronaviruses nsp14 in vitro when incubated with different compounds at 100  $\mu\text{M}$  using biochemical assays. As shown in Fig. 2A, sinefungin effectively inhibits the activities of all four N7-MTases and AdoHcy and ATA weakly inhibit the N7-MTase activities of SARS, MHV and TGEV with approximately 45–70% inhibition at 100  $\mu\text{M}$ , except for IBV with 10–30% inhibition.

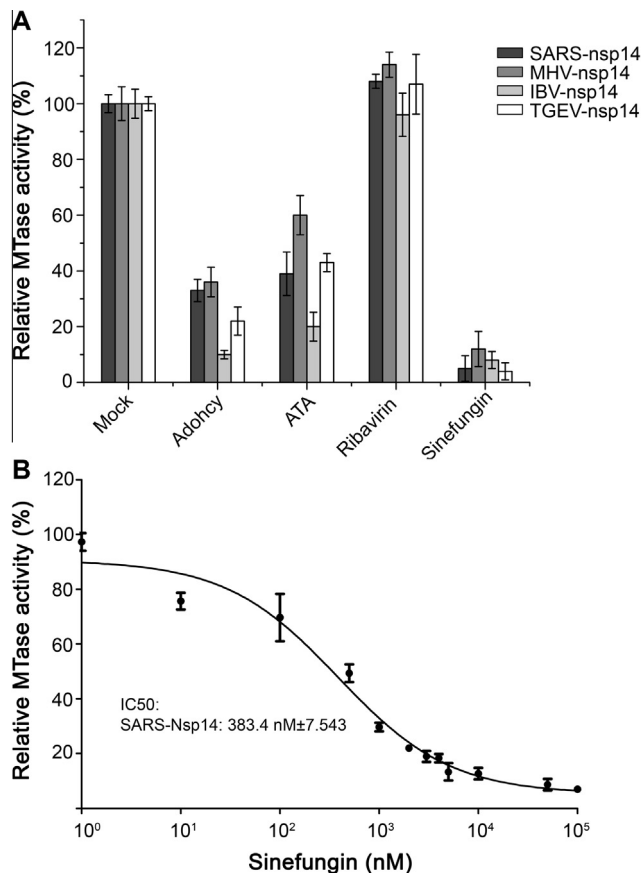


**Fig. 2.** Inhibitory effects of previously identified inhibitors on coronavirus N7-MTase activities in biochemical assays. (A) Four chemical compounds were tested for the inhibition of four coronavirus N7-MTases. Nsp14 (200 nM) was incubated with GpppA to detect methyl transfer to the substrates by a filter-binding assay (see Materials and Methods); methyl transfer was measured with each inhibitor at 100  $\mu\text{M}$ . The result of the control reaction with 1% DMSO instead of the inhibitor was set at 100%. The mean value of three independent experiments is given. (B) Dose–response curves and  $\text{IC}_{50}$  values of sinefungin on SARS nsp14 (N7-MTase). The results of three independent experiments with standard deviations are illustrated. The  $\text{IC}_{50}$  values were calculated as described in Materials and Methods.

In contrast, ribavirin, which is a guanosine (ribonucleic) analog used to interfere with viral RNA synthesis and viral mRNA capping of many different viruses (Kim and Lee, 2013; Scholtissek, 1976; Zhao et al., 2012), did not inhibited the coronavirus N7-MTases. The dose–response curve of sinefungin, which was the best inhibitor of the three effective compounds, showed an  $\text{IC}_{50}$  value of sinefungin against SARS-CoV nsp14 of  $383.4 \pm 7.54$  nM (Fig. 2B). Sinefungin could widely inhibit the activities of MTases from diverse sources including viruses and yeast. For example, the  $\text{IC}_{50}$  values of sinefungin for N7-MTase and 2'-O-MTases of Vaccinia virus in vitro are 12.0 and 39.5 nM, respectively (Pugh et al., 1978), and the  $\text{IC}_{50}$  values for 2'-O-MTase (NS5MTase) activity of Dengue virus in vitro are 420 nM (Li et al., 2007) and 630 nM (Selisko et al., 2010). The  $\text{IC}_{50}$  values of sinefungin for yeast N7-MTase are 55 nM in vivo (Chrebet et al., 2005) and 24 nM in vitro (Zheng et al., 2007), respectively. It was reported previously that the  $\text{IC}_{50}$  values of AdoHcy are 1 and 0.5 mM for N7-MTase and 2'-O-MTases activities of Vaccinia virus in vitro, respectively (Pugh and Borchardt, 1982). In this study, the inhibitory effects of sinefungin, AdoHcy and ATA on MTases were consistent with that of previous reports.

As sinefungin, AdoHcy and ATA were effective inhibitors of coronaviruses N7-MTases in biochemical assays, they were used to validate the yeast-based assay system established in this study (Fig. 3). The yeast strains MT-Yeast, MT-Human, and MT-SARS were incubated with 100  $\mu\text{M}$  of each compound, and the cell growth was measured at 4-h intervals over a 48-h period. Remarkably, sinefungin significantly repressed the growth of all three yeast strains (Fig. 3), confirming the previous report of sinefungin as a potent inhibitor (Chrebet et al., 2005; Li et al., 2007; Pugh et al., 1978). In contrast, ATA, AdoHcy, and ribavirin did not exhibit inhibitory activities against the three yeast strains. Because AdoHcy and ATA could inhibit the activity of coronavirus N7-MTase in biochemical assays, the results showed a clear difference between in vitro biochemical assays and in vivo cell-based assays, indicating that N7-MTase inhibitors identified using in vitro biochemical assays may not necessarily be effective within a cellular context. Such discrepancy may be attributed to the low membrane permeability to AdoHcy and ATA or that the  $\text{IC}_{50}$  of AdoHcy and ATA are far greater than 100  $\mu\text{M}$ . Indeed, sinefungin has been reported to be actively transported across yeast membranes, whilst AdoHcy and ATA are not (Zheng et al., 2006, 2007).

Sinefungin, which is produced by *Streptomyces*, is a natural sulfur-modified analog of AdoHcy, a well-characterized, nonspecific MTase inhibitor. As shown in Fig. 3, sinefungin exhibited a similar inhibitory effect on all three yeast strains at high concentration (100  $\mu\text{M}$ ). However, stronger inhibitory effect on MT-Yeast was observed than that on MT-Human and the strains harboring the MTases of other coronaviruses at low concentration (0.1  $\mu\text{M}$ ) (Fig. 4A and B). This could be explained by intrinsic difference of inhibitory effect to different MTases or the difference of the expression levels of the MTases as we showed that higher mRNA levels of MT-Human and MTases of coronaviruses were expressed than that of MT-yeast (Fig. 1C). To further characterize sinefungin as an MTase inhibitor in the yeast-based system, yeast strain YBS40, expressing different N7-MTases, was incubated with sinefungin at different concentration for 20 h (Fig. 4C and D). The  $\text{IC}_{50}$  ( $n = 3$ , mean values  $\pm$  SD) of MT-Yeast, MT-Human and MTases of coronaviruses were calculated and shown in Table 1. These results indicate that sinefungin is a broad-spectrum inhibitor against various species of N7-MTases, including those from yeasts, humans, and coronaviruses and demonstrate that the yeast-based system could be used for analysis of N7-MTase inhibitors. However, sinefungin is not an ideal antiviral inhibitor due to its lack of specificity on coronavirus N7-MTases compared to yeast and human MTases. Therefore, it is still necessary to screen for specific viral N7-MTases inhibitors, an

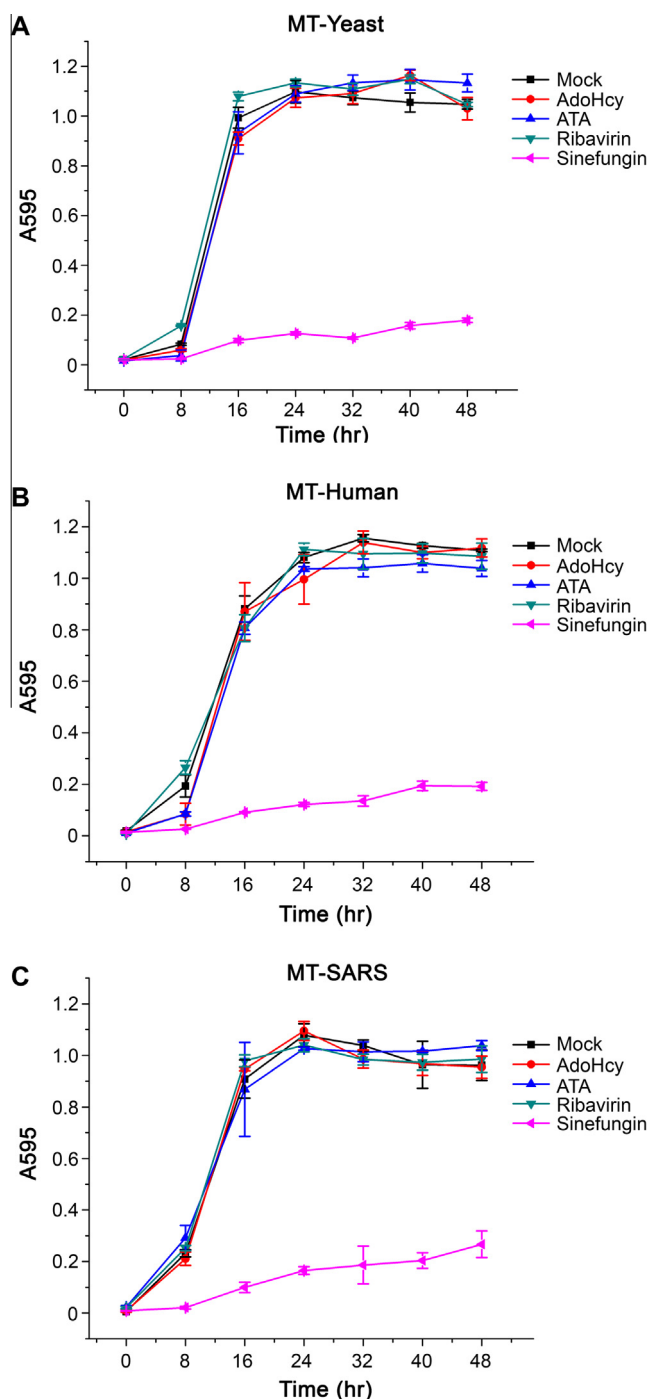


**Fig. 3.** Inhibitory effects of the compounds on the coronavirus N7-MTase-dependent yeast cell growth. Yeast cells were inoculated with 100  $\mu$ M of inhibitor candidates (AdoHcy, ATA, ribavirin, and sinefungin), and 1% DMSO was used as a control in the absence of inhibitor. The cell growth of the 1% DMSO control was set as 100%. The absorbance was measured spectrophotometrically at 595 nm. Black, mock; red, AdoHcy; blue, ATA; green, ribavirin; light red, sinefungin. (A) MT-Yeast, (B) MT-Human, and (C) MT-SARS. (For interpretation of the references to colour in this figure legend, the reader is referred to the web version of this article.)

effort that will benefit the functional study of viral MTases and clinical drug development.

### 3.3. Screening for effective microbial natural products using the yeast-based assay

As the three yeast strains, MT-Yeast, MT-Human, and MT-SARS, have the same genetic background and their growth depends on

yeast, human, and SARS-CoV MTases, respectively, the yeast-based system described above can be adopted to screen specific inhibitors against coronavirus N7-MTase. It is of note that the mRNA levels of MT-SARS and MT-Human are similar but they are higher than that of MT-yeast (Fig. 1C). However, this would not influence the screening for inhibitors with more specific inhibition on SARS-CoV MTase over human MTase.

For the screening of inhibitors to SARS-CoV N7-MTase, over 3000 microbial natural product extracts were tested in the yeast-based system. The microbial extracts were prepared from liquid culture of actinomycetes and fungi as described in the Materials and Methods section. The overnight cultures of MT-Yeast, MT-Human, and MT-SARS were diluted to  $A_{595} = 0.01$ , and a 100- $\mu$ L aliquot of each cell culture was seeded into 96-well microtiter plates in the presence of 30  $\mu$ g/ml of microbial natural product extract. Twenty hours post-incubation, the cell density was monitored by measuring the optical density at  $A_{595}$ . In the first round, the extracts that did not repress MT-Human were selected for further testing. The primary candidate extracts were tested twice for reproducibility and inhibitory effects using independent samples of each extract. In summary, we obtained three candidate extracts, PF35468 (natural product extract from a fungus species, preliminarily characterized as *Penicillium* spp.), PA48202 and PA48523 (natural product extracts from actinomycetes, preliminarily characterized as *Streptomyces* spp.), which could potentially inhibit the growth of MT-SARS and MT-yeast but significantly less effectively inhibit MT-Human (Fig. 5). The inhibition ratios of the 3 extracts on MT-SARS to MT-Human were 3.5, 3, and 9, respectively. In contrast, sinefungin suppressed the growth of all 3 yeast strains at a final concentration of 10  $\mu$ M (3.81  $\mu$ g/ml). The fungal and actinomycetes natural product extracts used in this study were composed of complex ingredients, and these three extracts could be used for the isolation of the active ingredients in future work. Taken together, the yeast-based assay system could provide a platform for screening N7-MTase inhibitors that are more effective against viral MTases and less effective against human MTases.

### 3.4. Optimizing the yeast-based assay for high-throughput screening

Efficient drug development often depends on high-throughput screening, which offers rapid and sensitive data acquisition coupled with high-content analyses. To explore the possibility of miniaturizing the yeast-based assay and to increase its throughput scale, yeast cells were seeded in 384-well microtiter plates, and the growth of the MT-SARS yeast cells was monitored at 4-h intervals over 48 h at 30  $^{\circ}$ C in a shaker (Fig. 6A and B). During the logarithmic growth phase (4–24 h), the optical density of the culture at  $A_{595}$  was well correlated with the cell number (Fig. 6A–C). The following linear regression equation was established for the MT-SARS strain:  $y = 8.82419x - 0.12315$  ( $R^2 = 0.992$ ), indicating that they are more correlative in 384-well microtiter plates than 96-well microtiter plates (Fig. 6C). To validate the yeast-based system for the high-throughput screening of inhibitors against N7-MTases, we performed a growth suppression assay and measured the  $IC_{50}$  of sinefungin against the 6 yeast strains that had been tested in the 96-well format (Fig. 6D and E). The  $IC_{50}$  values ( $n = 3$ , mean values  $\pm$  SD) for sinefungin against MT-Yeast, MT-Human, MT-SARS, MT-MHV, MT-TGEV, and MT-IBV were  $39.18 \pm 12.13$  nM,  $623 \pm 1.36$  nM,  $1621 \pm 2.14$  nM,  $1349 \pm 3.33$  nM,  $1398 \pm 1.34$  nM, and  $1430 \pm 4.87$  nM, respectively (Table 1), which were highly consistent with that of the 96-well microtiter plates (Figs. 4 and 6 and Table 1). These results indicate that the yeast-based high-throughput screening system could be used for the discovery of specific antiviral inhibitors. In comparison to the 96-well microplate assays, the 384-well assay system was more reliable, and cost effective.

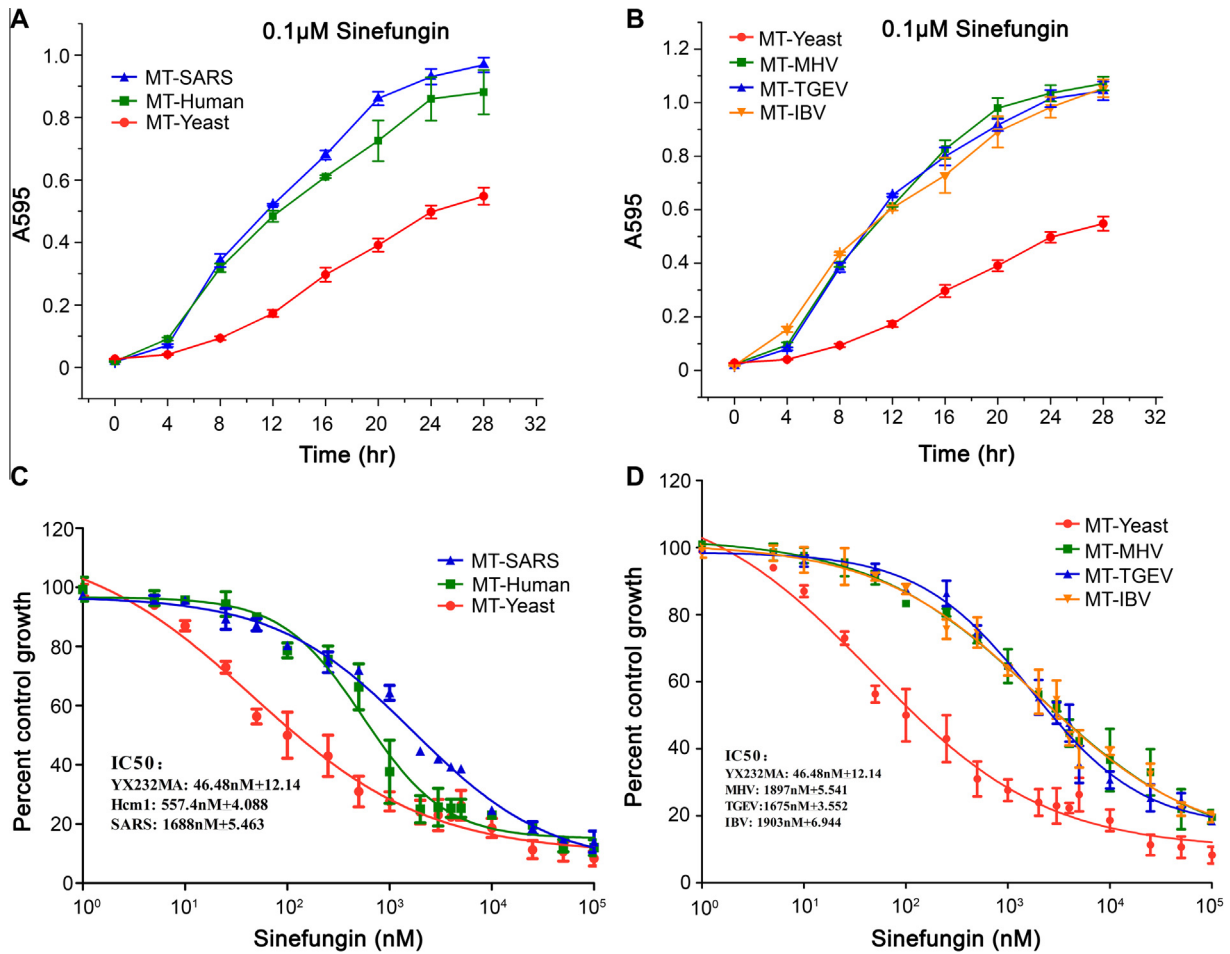


**Fig. 4.** Evaluation of the inhibitory effects of sinefungin in yeast-based assays. (A and B) The growth curve of the yeast strains carrying MT-Yeast, MT-Human, MT-SARS and MTases from other coronaviruses with 0.1  $\mu$ M sinefungin. (C and D) The IC<sub>50</sub> value of sinefungin was determined for the six YBS40 strains expressing human, yeast, SARS, MHV, TGEV, and IBV N7-MTases (MT-Human, MT-Yeast, MT-SARS, MT-MHV, MT-TGEV, and MT-IBV). The mean values with standard deviations of six repeats are indicated.

**Table 1**  
IC<sub>50</sub> values of sinefungin against the N7-MTases in yeast cells.

N7-MTases	IC <sub>50</sub>	
	96 well-plate	384 well-plate
MT-Yeast	46.48 nM ± 12.14 <sup>a</sup>	39.18 nM ± 12.13
MT-Human	557.40 nM ± 4.088	623.60 nM ± 1.359
MT-SARS	1688.00 nM ± 5.463	1621.00 nM ± 2.136
MT-MHV	1897.00 nM ± 5.541	1349.00 nM ± 3.328
MT-TGEV	1675.00 nM ± 3.552	1398.00 nM ± 1.338
MT-IBV	1903.00 nM ± 6.944	1430.00 nM ± 4.869

<sup>a</sup> The numbers represent the mean ± standard deviations (SD) with  $n = 6$ .

#### 4. Discussion

Many coronaviruses cause severe human and animal diseases. Recently, a novel SARS-like coronavirus, the Middle East respiratory syndrome coronavirus (MERS-CoV) belonging to the genus Betacoronavirus, was identified in Saudi Arabia and subsequently spread to the United Kingdom (UK), Germany, and France (Al-Tawfiq, 2013; Lim et al., 2013; Wiwanitkit, 2014). As there are no clinically approved antiviral therapies, including effective antiviral drugs, available to date for the treatment of coronavirus-associated diseases, the establishment of a high-throughput antiviral inhibitor screening system is important for the development of novel anti-coronavirus drugs.

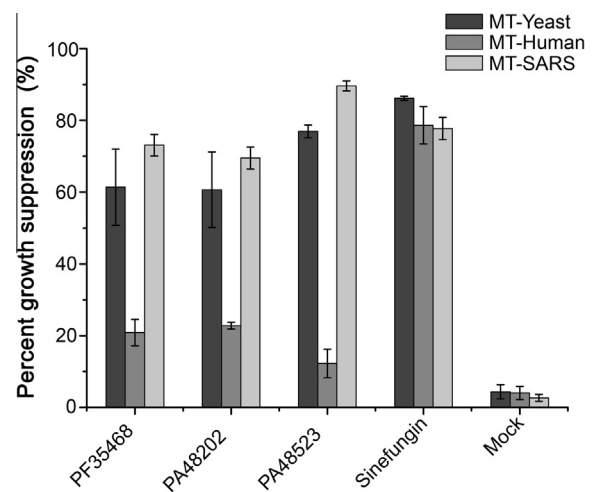


**Fig. 5.** The inhibitory effects of microbial natural product extracts screened using the yeast-based system. Sinefungin as an N7-MTase inhibitor was used as a positive control, and yeast culture in the absence of extracted compounds was used as the mock control. PF35468, PA48202, and PA48523 represent the three microbial natural product extracts. The growth suppression in percentage was calculated as  $[(X - Y)/X] \times 100\%$  where  $X$  is the  $A_{595}$  value of the mock culture and  $Y$  is the  $A_{595}$  value in the presence of sinefungin or microbial natural product extracts. The experiments were repeated three times. The results are shown as the percent suppression of cell growth of yeast strains MT-SARS, MT-human, and MT-Yeast.

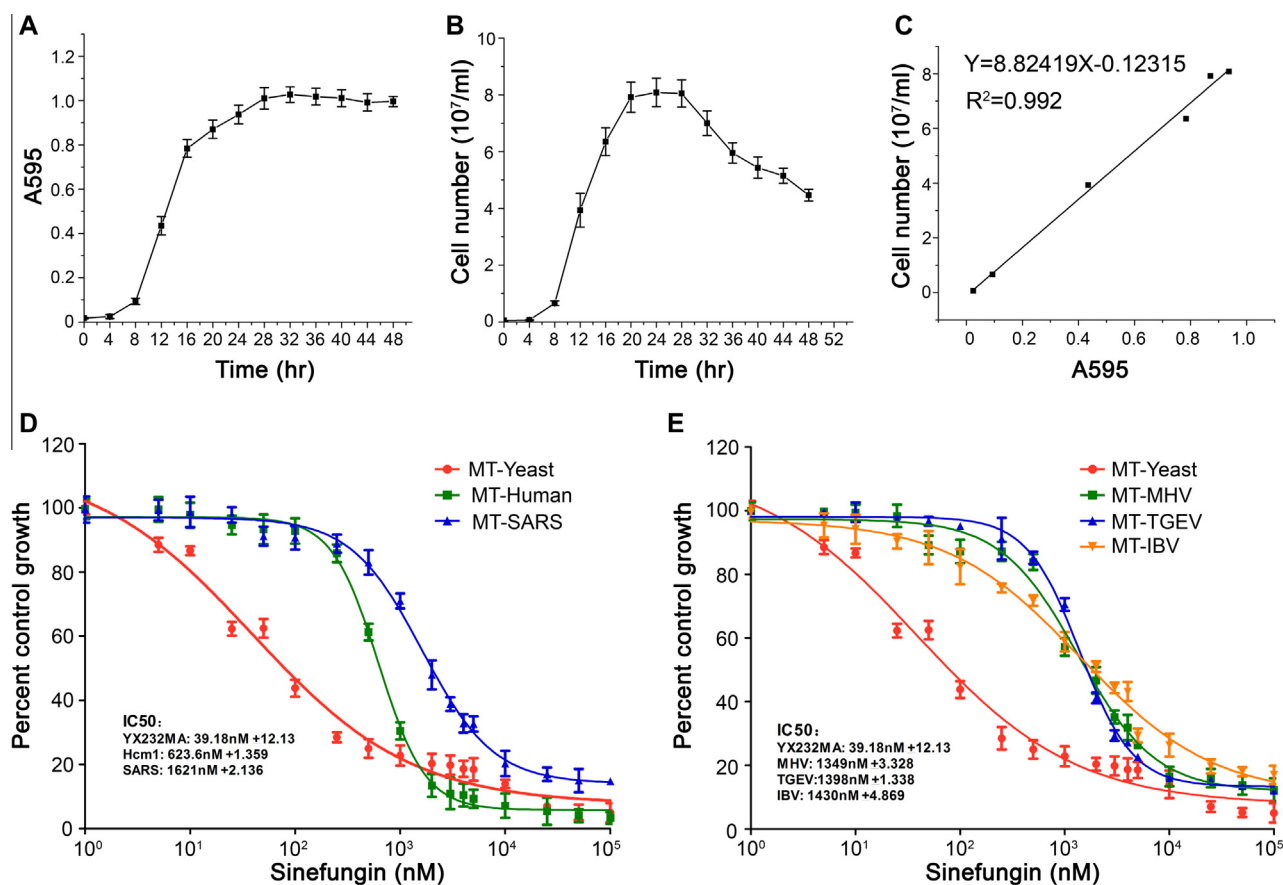


**Fig. 6.** Yeast-based assays of N7-MTase inhibitors in 384-well microtiter plates. (A) The spectrophotometric values of cell density in MT-SARS and (B) cell number in MT-SARS were plotted. (C) The linear regression of the optical density and cell number in the logarithmic phase (4–24 h) was  $y = 8.82419x - 0.12315$  ( $R^2 = 0.992$ ). (D and E) The dose-response curves and  $IC_{50}$  values of sinefungin against MT-Yeast, MT-Human, MT-SARS, MT-MHV, MT-TGEV, and MT-IBV were determined. The results of three independent experiments are shown, and the  $IC_{50}$  values were calculated as described in Materials and Methods.

Although AdoHcy, ATA and sinefungin, were previously reported to be inhibitors of coronavirus RNA MTases in vitro (Bouvet et al., 2010), only sinefungin significantly suppressed the growth of the MT-yeast, MT-human, and MT-SARS yeast cells (Fig. 3). Among these three strains, sinefungin was more effective against MT-Yeast than MT-SARS (Fig. 4). Thus, the observed differences between in vitro biochemical assays and yeast-based assays indicate that the inhibitors identified by an in vitro biochemical assay may not be effective in cells. As the yeast cell-based assay system is more similar to host cells with regard to the complexity of chemical composition than an in vitro biochemical assay, the former may have advantages over the latter for the identification of antiviral inhibitors that can function effectively in living cells.

Although the yeast-based N7-MTase assay system was validated by testing previously identified inhibitors, no specific inhibitors against coronavirus N7-MTases were identified. As the yeast-based system developed in this study included three yeast strains carrying yeast, human, or coronavirus N7-MTase activity, this method could be used to screen and identify inhibitors that are specific against coronaviruses and not (or significantly less effective) to human N7-MTase. In addition, the structural and mechanistic differences among coronavirus, yeast, and human MTases also provide the rationale for developing specific inhibitors. Accordingly, we exploited these differences and screened over 3000 natural product extracts. Interestingly, three extracts showed more potent inhibitory effects on SARS-CoV and yeast N7-MTase than human N7-MTase (Fig. 5).

A useful drug screening system should be able to be operated in a high-throughput manner. Therefore, the yeast cell-based system

of this study was optimized for 384-well microtiter plates. In this system, the yeast cells grew well and did not sediment (Fig. 6). Currently, only the AdoMet and AdoHcy backbones are used to synthesize analogs for the development of inhibitors that are specific for viral N7-MTases (Lim et al., 2011). The high-throughput yeast-based platform makes it possible to screen a large number of natural product extracts. The yeast-based system can be further used to screen a chemically synthesized compound library. The compounds obtained from such screenings may contribute to the drug design and development needed for the control of coronaviruses.

## Acknowledgments

We thank Dr. S. Shuman for kindly providing the yeast plasmids and strains and Dr. Eric J. Snijder for the IBV-nsp14 *E. coli* expression plasmid. We are grateful to Dr. Luis. Enjuanes for providing the China “973” Basic Research Program (2010CB911800 and 2013CB911101), China NSFC grants (81130083, 31170152, 81271817, and 31221061) and China Specialized Research Fund for the Doctoral Program of Higher Education (20120141130008). D.G. is supported by Hubei Province’s Outstanding Medical Academic Leader Program.

## References

- Abbas, Y.M., Pichlmair, A., Gorna, M.W., Superti-Furga, G., Nagar, B., 2013. Structural basis for viral 5'-PPP-RNA recognition by human IFIT proteins. *Nature* 494, 60–64.
- Al-Tawfiq, J.A., 2013. Middle east respiratory syndrome-coronavirus infection: An overview. *J. Infect. Public Health* 6, 319–322.

- Bouvet, M., Debarnot, C., Imbert, I., Selisko, B., Snijder, E.J., Canard, B., Decroly, E., 2010. In vitro reconstitution of SARS-coronavirus mRNA cap methylation. *PLoS Pathog.* 6, e1000863.
- Bowzard, J.B., Ranjan, P., Sambhara, S., 2013. RIG-I goes beyond naked recognition. *Cell Host Microbe* 13, 247–249.
- Chang, G.H., Luo, B.J., Lu, P., Lin, L., Wu, X.Y., Li, J., Hu, Y., Zhu, Q.Y., 2011. Construction and genetic analysis of murine hepatitis virus strain A59 Nsp16 temperature sensitive mutant and the revertant virus. *Virology* 436, 19–29.
- Chen, P., Jiang, M., Hu, T., Liu, Q., Chen, X.S., Guo, D., 2007. Biochemical characterization of exoribonuclease encoded by SARS coronavirus. *J. Biochem. Mol. Biol.* 40, 649–655.
- Chen, Y., Cai, H., Pan, J., Xiang, N., Tien, P., Ahola, T., Guo, D., 2009. Functional screen reveals SARS coronavirus nonstructural protein nsp14 as a novel cap N7 methyltransferase. *Proc. Natl. Acad. Sci. U.S.A.* 106, 3484–3489.
- Chen, Y., Su, C., Ke, M., Jin, X., Xu, L., Zhang, Z., Wu, A., Sun, Y., Yang, Z., Tien, P., Ahola, T., Liang, Y., Liu, X., Guo, D., 2011. Biochemical and structural insights into the mechanisms of SARS coronavirus RNA ribose 2'-O-methylation by nsp16/nsp10 protein complex. *PLoS Pathog.* 7, e1002294.
- Chen, Y., Tao, J., Sun, Y., Wu, A., Su, C., Gao, G., Cai, H., Qiu, S., Wu, Y., Ahola, T., Guo, D., 2013. Structure-function analysis of severe acute respiratory syndrome coronavirus RNA cap guanine-N7-methyltransferase. *J. Virol.* 87, 6296–6305.
- Chretien, G.L., Wisniewski, D., Perkins, A.L., Deng, Q., Kurtz, M.B., Marcy, A., Parent, S.A., 2005. Cell-based assays to detect inhibitors of fungal mRNA capping enzymes and characterization of sinefungin as a cap methyltransferase inhibitor. *J. Biomol. Screen.* 10, 355–364.
- Daffis, S., Szretter, K.J., Schriever, J., Li, J., Youn, S., Errett, J., Lin, T.Y., Schneller, S., Züst, R., Dong, H., Thiel, V., Sen, G.C., Fensterl, V., Klimstra, W.B., Pierson, T.C., Buller, R.M., Gale Jr., M., Shi, P.Y., Diamond, M.S., 2010. 2'-O methylation of the viral mRNA cap evades host restriction by IFIT family members. *Nature* 468, 452–456.
- Darnell Jr., J.E., 1979. Transcription units for mRNA production in eukaryotic cells and their DNA viruses. *Prog. Nucleic Acid Res. Mol. Biol.* 22, 327–353.
- de Groot, R.J., Baker, S.C., Baric, R.S., Brown, C.S., Drosten, C., Enjuanes, L., Fouchier, R.A., Galiano, M., Gorbalenya, A.E., Memish, Z.A., Perlman, S., Poon, L.L., Snijder, E.J., Stephens, G.M., Woo, P.C., Zaki, A.M., Zambon, M., Ziebuhr, J., 2013. Middle east respiratory syndrome coronavirus (MERS-CoV): announcement of the coronavirus study group. *J. Virol.* 87, 7790–7792.
- Decroly, E., Debarnot, C., Ferron, F., Bouvet, M., Coutard, B., Imbert, I., Gluais, L., Papageorgiou, N., Sharff, A., Bricogne, G., Ortiz-Lombardia, M., Lescar, J., Canard, B., 2011. Crystal structure and functional analysis of the SARS-coronavirus RNA cap 2'-O-methyltransferase nsp10/nsp16 complex. *PLoS Pathog.* 7, e1002059.
- Decroly, E., Imbert, I., Coutard, B., Bouvet, M., Selisko, B., Alvarez, K., Gorbalenya, A.E., Snijder, E.J., Canard, B., 2008. Coronavirus nonstructural protein 16 is a cap-0 binding enzyme possessing (nucleoside-2'-O)-methyltransferase activity. *J. Virol.* 82, 8071–8084.
- Filipowicz, W., Furuichi, Y., Sierra, J.M., Muthukrishnan, S., Shatkin, A.J., Ochoa, S., 1976. A protein binding the methylated 5'-terminal sequence, m7G pppN, of eukaryotic messenger RNA. *Proc. Natl. Acad. Sci. U.S.A.* 73, 1559–1563.
- Furuichi, Y., Shatkin, A.J., 2000. Viral and cellular mRNA capping: past and prospects. *Adv. Virus Res.* 55, 135–184.
- Ho, C.K., Martins, A., Shuman, S., 2000. A yeast-based genetic system for functional analysis of viral mRNA capping enzymes. *J. Virol.* 74, 5486–5494.
- Hornung, V., Ellegast, J., Kim, S., Brzozka, K., Jung, A., Kato, H., Poeck, H., Akira, S., Conzelmann, K.K., Schlee, M., Endres, S., Hartmann, G., 2006. 5'-Triphosphate RNA is the ligand for RIG-I. *Science* 314, 994–997.
- Hussain, S., Pan, J., Chen, Y., Yang, Y., Xu, J., Peng, Y., Wu, Y., Li, Z., Zhu, Y., Tien, P., Guo, D., 2005. Identification of novel subgenomic RNAs and noncanonical transcription initiation signals of severe acute respiratory syndrome coronavirus. *J. Virol.* 79, 5288–5295.
- Kim, Y., Lee, C., 2013. Ribavirin efficiently suppresses porcine nidovirus replication. *Virus Res.* 171, 44–53.
- Li, J., Chorbha, J.S., Whelan, S.P., 2007. Vesicular stomatitis viruses resistant to the methylase inhibitor sinefungin upregulate RNA synthesis and reveal mutations that affect mRNA cap methylation. *J. Virol.* 81, 4104–4115.
- Lim, P.L., Lee, T.H., Rowe, E.K., 2013. Middle east respiratory syndrome coronavirus (MERS CoV): update 2013. *Curr. Infect. Dis. Rep.* 15, 295–298.
- Lim, S.P., Sonntag, L.S., Noble, C., Nilar, S.H., Ng, R.H., Zou, G., Monaghan, P., Chung, K.Y., Dong, H., Liu, B., Bodenreider, C., Lee, G., Ding, M., Chan, W.L., Wang, G., Jian, Y.L., Chao, A.T., Lescar, J., Yin, Z., Vedananda, T.R., Keller, T.H., Shi, P.Y., 2011. Small molecule inhibitors that selectively block dengue virus methyltransferase. *J. Biol. Chem.* 286, 6233–6240.
- Liu, H., Kiledjian, M., 2006. Decapping the message: a beginning or an end. *Biochem. Soc. Trans.* 34, 35–38.
- Lugari, A., Betzi, S., Decroly, E., Bonnaud, E., Hermant, A., Guillemot, J.C., Debarnot, C., Borg, J.P., Bouvet, M., Canard, B., Morelli, X., Lecine, P., 2010. Molecular mapping of the RNA Cap 2'-O-methyltransferase activation interface between severe acute respiratory syndrome coronavirus nsp10 and nsp16. *J. Biol. Chem.* 285, 33230–33241.
- Luzhkov, V.B., Selisko, B., Nordqvist, A., Peyrane, F., Decroly, E., Alvarez, K., Karlen, A., Canard, B., Qvist, J., 2007. Virtual screening and bioassay study of novel inhibitors for dengue virus mRNA cap (nucleoside-2'-O)-methyltransferase. *Bioorg. Med. Chem.* 15, 7795–7802.
- Mao, X., Schwer, B., Shuman, S., 1995. Yeast mRNA cap methyltransferase is a 50-kilodalton protein encoded by an essential gene. *Mol. Cell. Biol.* 15, 4167–4174.
- Milani, M., Mastrangelo, E., Bollati, M., Selisko, B., Decroly, E., Bouvet, M., Canard, B., Bolognesi, M., 2009. Flaviviral methyltransferase/RNA interaction: structural basis for enzyme inhibition. *Antiviral Res.* 83, 28–34.
- Minskaia, E., Hertzog, T., Gorbalenya, A.E., Campanacci, V., Cambillau, C., Canard, B., Ziebuhr, J., 2006. Discovery of an RNA virus 3' → 5' exoribonuclease that is critically involved in coronavirus RNA synthesis. *Proc. Natl. Acad. Sci. U.S.A.* 103, 5108–5113.
- Nallagatla, S.R., Toroney, R., Bevilacqua, P.C., 2008. A brilliant disguise for self RNA: 5'-end and internal modifications of primary transcripts suppress elements of innate immunity. *RNA Biol.* 5, 140–144.
- Pugh, C.S., Borchardt, R.T., 1982. Effects of S-adenosylhomocysteine analogues on vaccinia viral messenger ribonucleic acid synthesis and methylation. *Biochemistry* 21, 1535–1541.
- Pugh, C.S., Borchardt, R.T., Stone, H.O., 1978. Sinefungin, a potent inhibitor of virion mRNA(guanine-7)-methyltransferase, and viral multiplication. *J. Biol. Chem.* 253, 4075–4077.
- Rehwinkel, J., Tan, C.P., Goubau, D., Schulz, O., Pichlmair, A., Bier, K., Robb, N., Vreede, F., Barclay, W., Fodor, E., Reis e Sousa, C., 2010. RIG-I detects viral genomic RNA during negative-strand RNA virus infection. *Cell* 140, 397–408.
- Saha, N., Schwer, B., Shuman, S., 1999. Characterization of human, *Schizosaccharomyces pombe*, and *Candida albicans* mRNA cap methyltransferases and complete replacement of the yeast capping apparatus by mammalian enzymes. *J. Biol. Chem.* 274, 16553–16562.
- Saha, N., Shuman, S., Schwer, B., 2003. Yeast-based genetic system for functional analysis of poxvirus mRNA cap methyltransferase. *J. Virol.* 77, 7300–7307.
- Schibler, U., Perry, R.P., 1977. The 5'-termini of heterogeneous nuclear RNA: a comparison among molecules of different sizes and ages. *Nucleic Acids Res.* 4, 4133–4149.
- Scholtissek, C., 1976. Inhibition of influenza RNA synthesis by virazole (ribavirin). *Arch. Virol.* 50, 349–352.
- Schwer, B., Lehman, K., Saha, N., Shuman, S., 2001. Characterization of the mRNA capping apparatus of *Candida albicans*. *J. Biol. Chem.* 276, 1857–1864.
- Schwer, B., Mao, X., Shuman, S., 1998. Accelerated mRNA decay in conditional mutants of yeast mRNA capping enzyme. *Nucleic Acids Res.* 26, 2050–2057.
- Selisko, B., Peyrane, F.F., Canard, B., Alvarez, K., Decroly, E., 2010. Biochemical characterization of the (nucleoside-2'-O)-methyltransferase activity of dengue virus protein NS5 using purified capped RNA oligonucleotides (7Me)GpppAC(n) and GpppAC(n). *J. Gen. Virol.* 91, 112–121.
- Shuman, S., 2001. Structure, mechanism, and evolution of the mRNA capping apparatus. *Prog. Nucleic Acid Res. Mol. Biol.* 66, 1–40.
- Sikorski, R.S., Boeke, J.D., 1991. In vitro mutagenesis and plasmid shuffling: from cloned gene to mutant yeast. *Methods Enzymol.* 194, 302–318.
- Snijder, E.J., Bredenoord, P.J., Dobbe, J.C., Thiel, V., Ziebuhr, J., Poon, L.L., Guan, Y., Rozanov, M., Spaan, W.J., Gorbalenya, A.E., 2003. Unique and conserved features of genome and proteome of SARS-coronavirus, an early split-off from the coronavirus group 2 lineage. *J. Mol. Biol.* 331, 991–1004.
- Weiss, S.R., Navas-Martin, S., 2005. Coronavirus pathogenesis and the emerging pathogen severe acute respiratory syndrome coronavirus. *Microbiol. Mol. Biol. Rev.* 69, 635–664.
- Wiwanitkit, V., 2014. Novel middle east respiratory syndrome coronavirus. *J. Formos. Med. Assoc.* 113, 65.
- Woyciniuk, P., Linder, M., Scholtissek, C., 1995. The methyltransferase inhibitor neplanocin A interferes with influenza virus replication by a mechanism different from that of 3-deazaadenosine. *Virus Res.* 35, 91–99.
- Zaki, A.M., van Boheemen, S., Bestebroer, T.M., Osterhaus, A.D., Fouchier, R.A., 2012. Isolation of a novel coronavirus from a man with pneumonia in Saudi Arabia. *N. Engl. J. Med.* 367, 1814–1820.
- Zhao, L.J., Wang, W., Liu, Y., Ren, H., Qi, Z.T., 2012. Interference with ERK and STAT signaling pathways and inhibition of hepatitis C virus replication by ribavirin. *Antiviral Res.* 96, 260–268.
- Zheng, S., Hausmann, S., Liu, Q., Ghosh, A., Schwer, B., Lima, C.D., Shuman, S., 2006. Mutational analysis of *Encephalitozoon cuculic* mRNA cap (guanine-N7) methyltransferase, structure of the enzyme bound to sinefungin, and evidence that cap methyltransferase is the target of sinefungin's antifungal activity. *J. Biol. Chem.* 281, 35904–35913.
- Zheng, S., Shuman, S., Schwer, B., 2007. Sinefungin resistance of *Saccharomyces cerevisiae* arising from Sam3 mutations that inactivate the AdoMet transporter or from increased expression of AdoMet synthase plus mRNA cap guanine-N7 methyltransferase. *Nucleic Acids Res.* 35, 6895–6903.
- Ziebuhr, J., Snijder, E.J., Gorbalenya, A.E., 2000. Virus-encoded proteinases and proteolytic processing in the Nidovirales. *J. Gen. Virol.* 81, 853–879.
- Züst, R., Cervantes-Barragan, L., Habjan, M., Maier, R., Neuman, B.W., Ziebuhr, J., Szretter, K.J., Baker, S.C., Barchet, W., Diamond, M.S., Siddell, S.G., Ludewig, B., Thiel, V., 2011. Ribose 2'-O-methylation provides a molecular signature for the distinction of self and non-self mRNA dependent on the RNA sensor Mda5. *Nat. Immunol.* 12, 137–143.